Hysteretic structural changes within five-layered modulated 10M martensite of Ni–Mn–Ga(–Fe)

Vertát P., Seiner H., Straka L., Klicpera M., Sozinov A., Fabelo O., Heczko O.

DOI: 10.1088/1361-648X/abfb8f

Hysteretic structural changes within five-layered modulated 10M martensite of Ni-Mn-Ga(-Fe)

P. Veřtát[1,2,], H. Seiner[3], L. Straka[1,4], M. Klicpera[4], A. Sozinov[5], O. Fabelo[6], O. Heczko[1]*

[1] *FZU - Institute of Physics of the Czech Academy of Sciences, Na Slovance 1999/2, 18221 Prague 8, Czech Republic.*

[2] *Faculty of Nuclear Sciences and Physical Engineering, Czech Technical University in Prague, Trojanova 13, 11519 Prague 1, Czech Republic.*

[3] *Institute of Thermomechanics of the Czech Academy of Sciences, Dolejškova 1402/8, 18200 Prague 8, Czech Republic.*

[4] *Faculty of Mathematics and Physics, Charles University, Ke Karlovu 5, 12116 Prague 2, Czech Republic.*

[5] *Material Physics Laboratory, LUT University, Yliopistonkatu 34, 53850 Lappeenranta, Finland.*

[6] *Institut Laue-Langevin, 71 avenue des Martyrs, CS 20156, 38042 Grenoble cedex 9, France.*

*Corresponding author, *address:* Institute of Physics of the Czech Academy of Sciences, Na Slovance 1999/2, 18221 Prague 8, Czech Republic; *tel.:* +420 266 052714, *e-mail:* vertat@fzu.cz

Abstract

Modulated structure of Ni-Mn-Ga–based alloys is decisive in their magnetic shape memory functionality. However, the precise nature of their five-layered modulated 10M martensite is still an open question. We used X-ray and neutron diffraction experiments on single crystals to investigate structural changes within 10M-modulated martensite of the $Ni_{50}Mn_{27}Ga_{22}Fe_1$ magnetic shape memory alloy. The modulation vector gradually increases upon cooling from commensurate $\mathbf{q} = (2/5)\,\mathbf{g}_{110}$, where $\mathbf{g}_{110}$ is the reciprocal lattice vector, to incommensurate with $\mathbf{q}$ up to pseudo-commensurate $\mathbf{q} = (3/7)\,\mathbf{g}_{110}$. Upon heating, reverse changes are observed with a thermal hysteresis of ≈ 60 K. The same hysteretic behaviour was detected in the electrical resistivity and the effective elastic modulus. Scanning electron microscopy showed that the changes are accompanied by the refinement of the *a*/*b* laminate. These observations indicate that the commensurate state is a metastable form of 10M martensite. Upon cooling, this phase evolves through nanotwinning into a more irregular and more stable incommensurate structure.

Keywords: ferromagnetic shape memory, phase transformations, twinning, microstructure, structural modulation.

1. Introduction

Structural modulations, i.e., small periodic perturbations of atomic positions, are commonly observed in low temperature phases of (ferromagnetic) shape memory alloys [1–9]. Among these, Ni-Mn-Ga–based Heusler alloys are nowadays broadly studied for their magnetic shape memory (MSM) functionality and therefore possible applications in actuators and sensors [10–12]. In the single crystals of Ni-Mn-Ga alloys, three major martensitic phases were identified as non-modulated tetragonal martensite (NM) and five- (10M, previously also marked as 5M) and seven-layered (14M, previously also marked as 7M) modulated martensites [13–19]. The modulated phases possess extremely mobile twin boundaries. The single crystal of 10M phase exhibits magnetically induced reorientation (MIR) of ferroelastic (twin) domains in a moderate field of the order of 0.1 T [16,20–22] resulting in about 6 % magnetic field induced strain (MFIS) down to liquid helium temperature [23,24].

On the other hand, the NM phase exhibit no MIR in pure Ni-Mn-Ga. It has been suggested that the modulation-related atom displacement at twin boundaries creates diffuse interface [25] with flat energy landscape which contributes to the high mobility of the interface [26]. Similarly the easily displaced lattice planes across the modulation direction indicate very low shear modulus, which is also a factor considered to bring the high twin boundary mobility [27]. The decreased shear modulus in Ni-Mn-Ga-Co-Cu NM martensite [28] correlated with higher mobility of twin boundaries and appearance of MIR [29]. Thus, the modulation, either influencing the atomic structure of the twin boundary or relating to the low shear modulus, seem to be a critical factor for the high twin boundary mobility. In other words, the character of modulation, such as the degree of incommensurateness, or its evolution, may be of significant importance for the MIR and related MFIS and for the efficiency of the effects. Since the 10M martensite is much more abundant and seems closer to practical applications, we focus our discussion mainly on this phase.

Despite the apparent importance of modulation for extremely high twin boundary mobility, the precise nature of the 10M modulated martensite of the Ni-Mn-Ga–based alloys is still under discussion. Generally, the description of the modulation in Ni-Mn-Ga is usually based on long period stacking order where the shear displacement occurs on each basal plane along $(100)[1\bar{1}0]$ system with a periodicity equal to five or seven atomic layers for 10M and 14M respectively [13,30]; for close-to-stoichiometric Ni_2MnGa, in addition, 6M modulated premartensite may appear [31]. For a theoretical description of the modulations, two main concepts have been discussed: i) an *adaptive martensite model*, also referred to as the *nanotwinning model* (regarding the modulation as as *micro-* or *nanotwinned* stable martensitic phase), developed particularly for Ni-Al and Fe-Pd structures with martensitic transformation [32,33] and later applied on Ni_2MnGa [34–36]; and ii) the *wave modulation approach* i.e. usual general crystallographic approach considering that the atomic plane shifts vary in space following a displacement wave [37,38], also applied widely to Ni_2MnGa alloys [36,39–42].

Most of the studies concerning diffraction experiments on Ni-Mn-Ga–based alloys use the latter – the wave modulation approach. Within this concept, the modulation of 10M Ni-Mn-Ga martensite is described by a single modulation vector $\mathbf{q} = q\,\mathbf{g}_{110}$, where $\mathbf{g}_{110}$ is the [110]* reciprocal vector (using the monoclinic lattice inherited from the lattice of cubic austenite). The modulation was reported to be either *commensurate* (for non-stoichiometric Ni-Mn-Ga) with the modulation vector $\mathbf{q} = (2/5)\,\mathbf{g}_{110}$ [39,40,43], *incommensurate* with the irrational magnitude of the modulation vector q [36,39–43], or *pseudo-commensurate* with $\mathbf{q} \approx (3/7)\,\mathbf{g}_{110}$ (particularly for stoichiometric Ni_2MnGa) [39,40,42]. Furthermore, q varies between 2/5 and 3/7 for different compositions and temperatures [40,43].

Evaluation of the modulation vector **q** is usually based on the interpretation of the diffraction measurements of satellite reflections. The X-ray diffraction (XRD) and neutron diffraction (ND) experiments reported in the literature have been done mostly on polycrystalline samples. In this case, the ratio of the intensity of the modulation satellites to the background is usually unfavourable, not allowing precise examination. Hence, the higher orders of satellites are usually omitted, leading to potential misinterpretations. Single-crystal studies [36,42], on the other hand, reveal high-order (3+) satellite peaks of substantial intensity that advocate consideration of the stacking model of (220) in Ni-Mn-Ga martensites.

In the nanotwinning model, the modulated structures are described by a tetragonal or monoclinic lattice with an alternating sequence of nanotwins [34,44,45]. The 10M martensite is described as $(\bar{3}2)_2$ and 14M martensite as $(\bar{5}2)_2$ in Zhdanov notation (number marking the layers involved in nanotwin) [46,47]. Here, only two parameters are required for describing the modulated structure in the nanotwinning model: a tetragonal distortion of the nonmodulated unit cell and the stacking sequence. From the X-ray and neutron diffraction point of view, proving or disproving the nanotwinning model directly is difficult due to the required precise determination of atom positions in the 10M lattice, various twinning and extreme sensitivity of the structure to the mechanical stress, and/or imperfections of the single crystal resulting in peak broadening [48]. Here, indirect methods can bring some solutions. In the diffraction experiments based on the theory of Wang [49,50] and related SEM experiments, the nanotwinning on the scale less than 20 nm was found near the martensite transformation [51] as well as at low temperatures [52]. In previous TEM studies, the nanotwinned character of the structure was reasonably confirmed. The transition between 14M and nonmodulated tetragonal martensite occurred clearly by nanotwinning and moreover the 14M structure was characterized by many stacking faults indicating the irregularity of the structure [53]. The main strength of the nanotwinning model is that it directly relates the modulation to the non-linear elasticity theory of martensitic microstructures [54]. This enables the microstructures in modulated martensites to be treated as deeply hierarchical and built from NM tetragonal unit cells [44,55].

The combination of both approaches, the modulation-nanotwinning concept, was recently used for the theoretical explanation of the periodic modulations and the formation of 14M seven-layered modulated martensite [45]. Furthermore, Benešová et al. [56] proposed a theoretical model describing the evolution of irregular nanotwinning in 10M and 14M martensite and the transition between these modulated structures. According to this model, the irregularity and related incommensurateness increases due to changes in the energy landscape when approaching the intermartensitic transformation. Hence, the model brings a strong motivation for experimental studies of the evolution of the modulated structures close to the intermartensitic transition temperature. Observing an increase of irregularity in the modulation towards this temperature would support the idea that the modulations and the intermartensitic transition could be captured by models based on elastic energy minimization.

Other complementary methods can bring an additional insight into the temperature evolution of martensite. The resonant ultrasound spectroscopy (RUS [57,58]) method, being based on resonant frequencies, is extremely sensitive to very slight changes of microstructure or mechanical properties [59]. The method is quite often used for analyzing elastic anomalies such as shear phonon softening accompanying phase transitions in shape memory alloys, e.g. [60]. The elastic anomalies are closely related to the stability of the crystal lattice [61], while the transition from metastable to stable states is typically accompanied by elastic stiffening. In this sense, RUS helps us to understand the stability and metastability of the individual modulation states. Furthermore, the electrical resistivity measurements can provide insight into the changes of transport properties during the (inter)martensitic transformations.

This paper presents a complex study of the hysteretic structural changes within five-layered modulated 10M martensite of $Ni_{50}Mn_{27}Ga_{22}Fe_1$ single crystal. In our neutron and X-ray diffraction experiments, we observed a hysteretic behaviour of the **q**-vector upon cooling and heating. This transition was also detectable by the electrical resistivity but not by magnetic susceptibility, and it is accompanied by significant changes of elastic properties observed by resonant ultrasound spectroscopy.

Our work can promote the discussion about the legitimacy of calling the 10M martensite of MSM alloys an invariable modulated phase in the whole temperature region of its existence. This deeply rooted idea is based on the diffraction measurements, which represent the averaging over the larger volume of the sample. Instead, our findings suggest that the 10M martensite might represent a metastable phase that, due to the irregular nanotwinning, is gradually evolving on a scale that is not directly accessible by the standard diffraction techniques.

2. Experimental

2.1 Samples, transformation temperatures, electrical resistivity, and SEM

We investigated a $Ni_{50}Mn_{27}Ga_{22}Fe_1$ single crystal produced by AdaptaMat Ltd. Two samples in the shape of rectangular prisms were cut from the single crystal ingot with faces along the {100} planes of cubic austenite. At room temperature, the samples exhibited the 10M modulated martensite structure. For X-ray and neutron diffraction, electrical resistivity measurements, and scanning electron microscopy, we used a sample of dimensions 13.0 × 2.6 × 0.9 mm^3 compressed along the long axis prior to the measurements. Such compression allowed us to obtain a single orientation of the short martensitic *c*-axis within the whole sample volume [62], simplifying the analysis of the martensite microstructure. For RUS and magnetic properties measurements, a smaller sample of dimensions 2.5 × 2.6 × 0.9 mm^3 was cut. In the usual monoclinic approximation using the lattice orientation inherited from austenite [17,39,40], the lattice parameters were determined as a = 0.5982 nm, b = 0.5945 nm, c = 0.5577 nm, γ = 90.3° by X-ray diffraction.

The structural and magnetic transformation temperatures were determined from the thermal dependence of the low field magnetization (DC susceptibility), Fig. 1, measured by the vibrating sample magnetometer (VSM) option of Quantum Design Physical Property Measurement System (PPMS) with the temperature rate of 4 K/min. From the measured curves, the transition temperatures were estimated as: martensitic transformation to 10M $T_{A\rightarrow 10M}$ = 328 K and reverse transformation $T_{10M\rightarrow A}$ = 337 K, and intermartensitic transformations $T_{10M\rightarrow 14M}$ = 200 K, $T_{14M\rightarrow NM}$ = 105 K, $T_{NM\rightarrow 14M}$ = 225 K, and $T_{14M\rightarrow 10M}$ = 280 K. The Curie temperature was estimated as T_C = 379 K. The doping of Ni-Mn-Ga by Fe led to an increase of magnetic and martensitic transformation temperatures, compared to other Ni-Mn-Ga systems [63–66], as expected. In the following text, we focus just on the temperature region of the stable 10M martensite (220 K – 330 K).

The temperature dependence of electrical resistivity within the 10M phase was measured in a Cryogenic cryostat with a closed cycle using custom-based measuring stage. The resistivity was measured by the AC four-point method (at frequency f = 11 Hz) using a Stanford Research Systems SR830 DSP Lock-In Amplifier, a Pico Precision PP102 current source, and a PP560 low noise amplifier.

Scanning electron microscope (SEM), TESCAN FERA3 GM iFIB-SEM, with a heating/cooling stage was used to confirm the sample stoichiometry and orientation. Back-scattered electrons (BSE) are sensitive to the crystallographic orientation of the lattice, and consequently to the different *a*/*b* twin variants due to the channelling contrast [67,68].

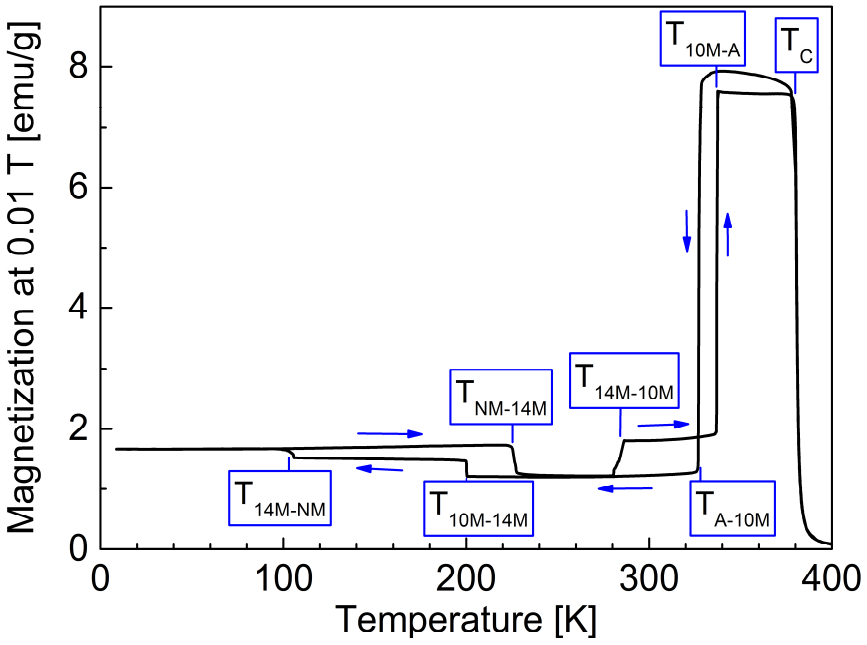

Fig. 1: DC magnetic susceptibility as a function of temperature. Transformation temperatures (martensitic transformation, intermartensitic transformations, and Currie point) are schematically marked.

2.2 X-ray and neutron diffraction

The XRD measurements were done on a Brucker D8 Discover diffractometer with a rotating Cu anode (λ = 0.1542 nm) equipped with Anton Paar DCS 350 cooling stage and a point detector. Neutron diffraction experiments were carried out on the D9 and D10 four-circle neutron diffractometers in ILL Grenoble (λ_{D9} = 0.0838 nm, λ_{D10} = 0.2360 nm), [dataset][69], [dataset][70], measuring primarily the q-scans. For both neutron experiments, the area detectors were used, allowing us to observe peaks from multiple martensite variants.

The modulation was evaluated using reciprocal space maps and q-scans at room temperature and at elevated and low temperatures. During the data processing, the detector area of the neutron data was carefully limited to exclude the possible differently oriented martensite variants from the integration and to obtain a high signal-to-noise ratio. Indexation was done following the previous reports by Fukuda et al. [42], Mariager et al. [36], and Righi et al. [40] using the wave modulation approach. The magnitude of the modulation vector was determined based on the relative positions of principal and satellite reflections. This ensures that the magnitude of the modulation vector is independent on the thermal expansion. Measured reflections were fitted employing the custom-made program FitExc [71]. To distinguish and match contributions from different mosaic blocks for each reflection (of the martensitic phases), the data were fitted using multiple peaks, allowing a precise calculation of the modulation vector. With this approach, we calculated the magnitudes of the modulation vector for each mosaic block separately and proved they were the same.

2.3 Resonant ultrasound spectroscopy (RUS)

We used a laser-based contactless modification of the RUS method [72], in which the vibrations of the sample are generated by a short (~ 10 ns nominal duration) pump laser pulse focused at one of the faces of the sample, and are recorded on another face of the sample by a laser vibrometer. This all-optical set-up enables the sample to be free from any clamping forces from the device, which significantly improves the accuracy and repeatability of the measurement.

The RUS spectra were measured in temperature intervals 322 K → 224 K → 325 K. The recorded spectra were in the frequency (f) range 50 – 500 kHz, sufficient to cover the lowest (up to 10) resonant modes. The sample was first measured in an as-prepared, poly-twinned condition, referred further as the *as-cut* condition. Subsequently, the sample was heated above the Curie point and then cooled down to room temperature in an external field of 1.1 T oriented along one edge of the sample, which resulted in a nearly single *c*-axis orientation state of the sample. Magnetization measurements confirmed that the sample after this treatment contained less than 10 % of the variants with the *c*-axis orientation different from the field orientation during the cooling. We will further refer to this condition as the *field-cooled* condition.

Due to the extremely high damping, only a very small number of resonant peaks was detectable in the RUS spectra, especially at the highest temperatures. This disabled a complete determination of the elastic constants. However, as utilized e.g. by Salje et al. [73] for twinned ferroelectric materials, and Kabla et al. [74] for sputtered SMA films, by plotting the temperature evolutions of the individual resonant frequencies, one can easily identify the phase transitions or other structural changes, as well as the precursor phenomena, such as phonon softening preceding the martensitic transitions [61]. Such an approach was also adopted in this work: we manually traced several resonant frequencies (with the number of traceable peaks varying in different temperature intervals depending on the damping) along the temperature cycle, which allowed us to reveal the general behavior of the elastic properties.

3. Results

Although the $Ni_{50}Mn_{27}Ga_{22}Fe_1$ exhibits a sequence of martensitic and intermartensitic transformations (Fig. 1), we have focused only on the temperature region of the stable 10M martensite (220 K – 330 K). Nevertheless, we have also examined the 14M and austenite phase of our sample and we did not find any difference to known literature. Therefore, the 14M or austenite phases will not be discussed in this paper. In our diffraction experiments, we found temperature-induced changes of the modulation vector **q** within the 10M martensite. We further examined the possible temperature evolution of the twinning microstructure, conductive, and elastic properties by SEM, electrical resistivity, and RUS.

3.1 Thermal evolution of 10M structure

To study the structural modulation, we performed the X-ray diffraction (XRD) and neutron diffraction (ND) experiments. These confirmed that the structure was modulated in the [110]* direction. Thus, our experiment could have been reduced to line q-scans (between (400) and (620), or (220) and (400) reflections) which revealed the full information about the modulation vector. Due to the sample compression prior to the measurement, the *c*-oriented martensite variant was not observed in the measured scans (out of the diffraction plane).

At the beginning, we have measured the q-scans by XRD at room temperature (preceded by cooling to 260 K to stabilize the phase) and at 328 K (just a few kelvins below the martensite-austenite transformation, $T_{10M\rightarrow A}$). We have found two contrasting patterns, clearly demonstrating the different character of 10M phase at room temperature (298 K) and at 328 K, Fig. 2.

We have analysed the detected satellite reflections following the usual wave-modulation approach as it is widely accepted by the shape memory community [36–42]. It warrants a straightforward interpretation and discussion of temperature-induced changes in the reciprocal space using well-established notation of one single parameter q. The analysis of the pattern obtained at room temperature (preceded by cooling to 260 K) revealed a complex modulated structure with *incommensurate* modulation, Fig. 2 a). In contrast, at 328 K the measurement indicates the commensurate 10M modulated structure ($\mathbf{q} = 0.400\ \mathbf{g}_{110}$), Fig. 2 b), with four equidistant satellite peaks between (400) and (620) reflections. The observed slight splitting of the peaks was caused by the mosaicity of the crystal and *a*/*b* twinning.

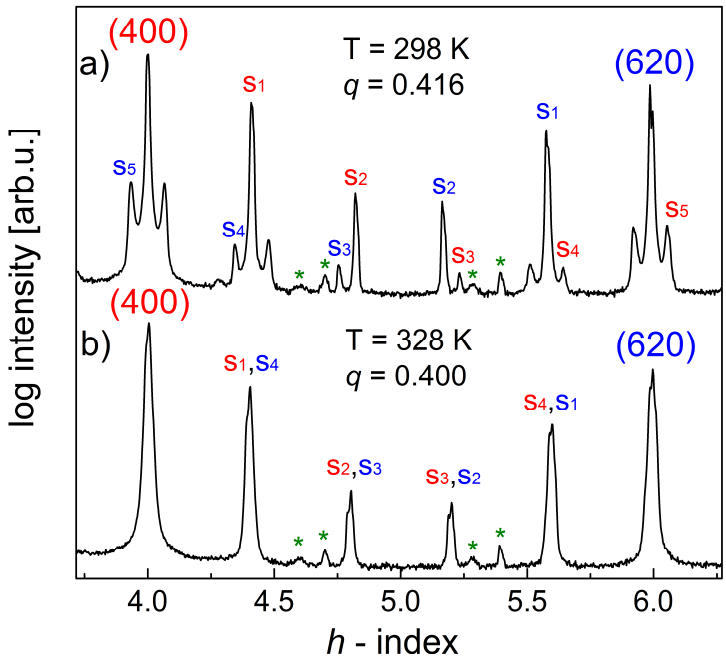

Fig. 2: q-scans in [110]* reciprocal direction determined by XRD: a) at 298 K (preceded by cooling to 260 K), b) after further heating to 328 K. Equidistant modulation satellites s_1...s_5 belonging to (400) and (620) reflections are marked red and blue, respectively. Reflections from the polycrystalline sample holder are marked with green asterisks.

Having obtained the above-described contrasting results, we measured q-scans by XRD in a wider temperature range with smaller steps during both heating and cooling. This revealed a significant shifting of the modulation satellites with temperature and related changes in q. At 220 K (few kelvins above the transition from 10M to 14M martensite, $T_{10M\rightarrow14M}$), the structure exhibited the *incommensurate* modulation with $q = 0.428(2)$. This approaches 3/7, corresponding to the *pseudo-commensurate* modulation found in stoichiometric Ni_2MnGa [36,39,42]. Further cooling to 210 K, not carried out in this run of the experiment, would result in an extensive change of the diffraction pattern connected with the intermartensitic transformation (IMT) to 14M martensite.

During the following heating, q decreased, reaching $q = 0.416(1)$ at room temperature. It further decreased with increasing temperature, attaining the exact value of $q = 0.400(1)$ at 328 K. The modulated structure thus became *commensurate*.

Importantly, during the following cooling from 328 K down to room temperature, the structure remained *commensurate* 10M. Only at 290 K, q started to increase again and the hysteretic behaviour was observed. The changes of modulation satellites in the measured q-scans are well visible in Fig. 3 for the region of hysteresis.

Aware of the fact that the XRD measurements are only surface layer sensitive (with a penetration depth of ~ 15 μm), we followed our experiments by bulk sensitive neutron diffraction (ND). We confirmed unambiguously that the modulation vector changed following the described scheme within the whole sample volume. The development of q with temperature (q-T diagram), as determined from XRD and ND, Fig. 4, shows an excellent agreement of both methods.

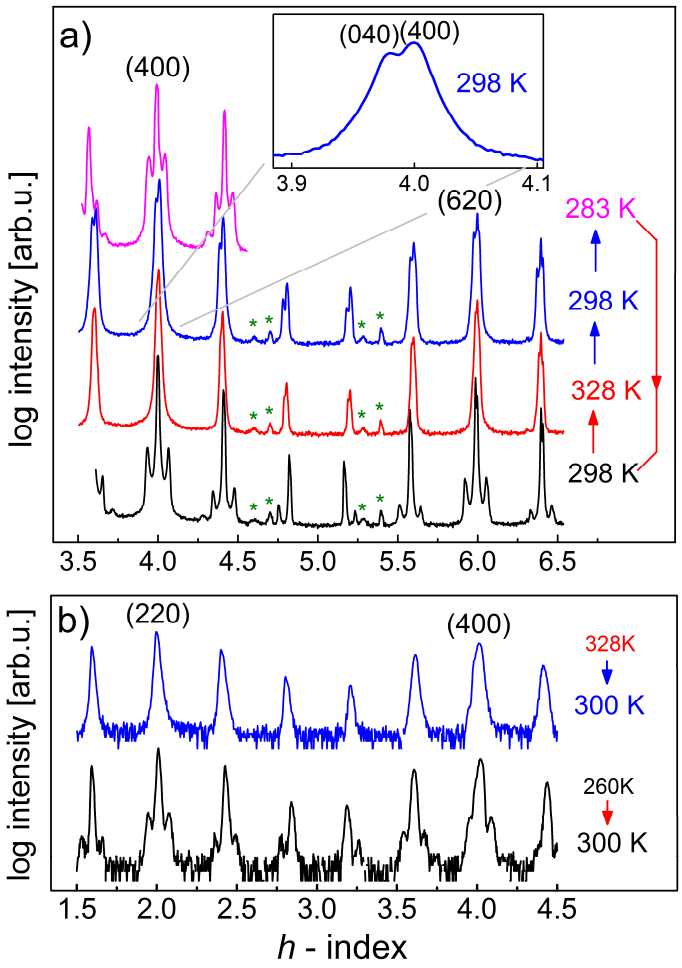

Fig. 3: Evolution of the diffraction pattern during thermal cycling as seen in q-scans along [110]* reciprocal direction obtained by a) XRD and b) ND. Owing to *a/b* twinning, both (400) and (040) reflections are present (zoomed in the inset). Reflections from the polycrystalline sample holder are marked with green asterisks.

Complementarily to the q-scans, we have measured simple XRD 2θ scans (not shown here). These indicated the refinement of the *a/b* twins down to nanoscale (but still larger than nanotwins) with decreasing temperature. In the *incommensurate* 10M phase, we observed only one reflection (400)', instead of two: (400) and (040), due to the refinement of the *a/b* twins. Such refinement has already been observed and discussed in [51,75]. For higher-temperature *commensurate* phase, the (400) and (040) reflections were clearly distinguished, indicating the relatively large *a/b* twin domains and thus well separated *a/b* twin boundaries. Simultaneously, the *a/b* twinning was apparent - the doubled peaks occurred in the above discussed q-scans. The separation between peaks became even larger when we cooled the sample back to room temperature (see the inset in Fig. 3), indicating the enlarged difference between *a* and *b* lattice constants [17]. The unchanged value of $q = 0.400(2)$ at room temperature was confirmed after we matched the related peaks.

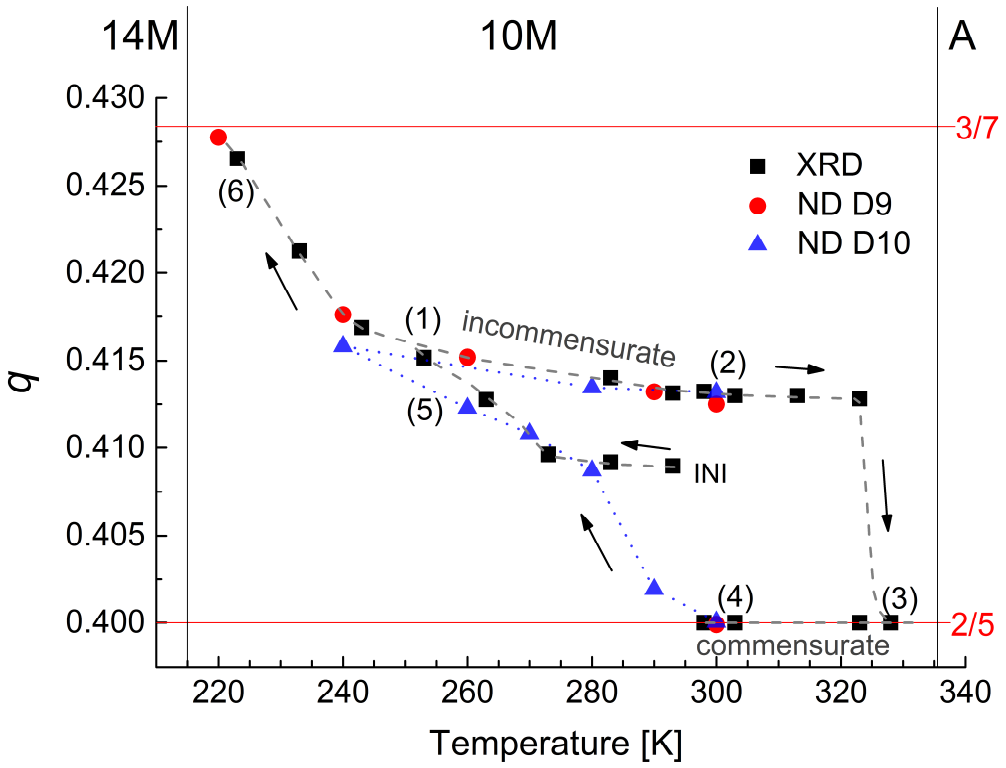

Fig. 4: Magnitude of the modulation vector q as a function of temperature. Black squares represent data from the XRD measurement, red circles and blue triangles stand for ND measurements on D9 and D10. Dotted and dashed lines connecting symbols from XRD and ND D10 runs are guides for the eyes. The arrows depict the sample heating/cooling cycles. Numbers in brackets refer to the SEM micrographs shown in Fig. 5. The point marked INI corresponds to the initial undefined state of the sample.

3.2 SEM observations and electrical resistivity

Direct confirmation of *a/b* twins refinement indicated by XRD came from scanning electron microscopy. The BSE micrographs, collected at six temperatures (Fig. 5; temperatures also marked in Fig. 4), revealed a clear horizontal band contrast corresponding to the *a/b* twin microstructure [68,76]. On cooling, the *a/b* twins became more refined, while on heating they became coarse again. This temperature evolution of the twin density showed about the same thermal hysteresis as q determined by XRD and ND (Fig. 4), that is, the twin refinement and changes in q are closely related. Heating the sample to austenite led to a disappearance of the band contrast (not shown), confirming that this contrast indeed originates from the *a/b* twinning.

Similar refinement of *a/b* twins was observed in Ni-Mn-Ga 10M martensite near the martensitic transformation [51] and also upon cooling [52]. The detailed analysis employing adaptive diffraction conditions and analysis of the SEM micrographs indicated the *mean width* of the *a/b* twins to be about 20 nm for nano-refined twins. We obtained similar micrographs and similar (400)-(040) peak merging as in [51] and thus we can ascribe them similar scales: ~150 nm twin width for coarse twins (cases (3) and (4) in Fig. 5) and <20 nm twin width for nanorefined twins (cases (1), (2), (5), (6) in Fig. 5).

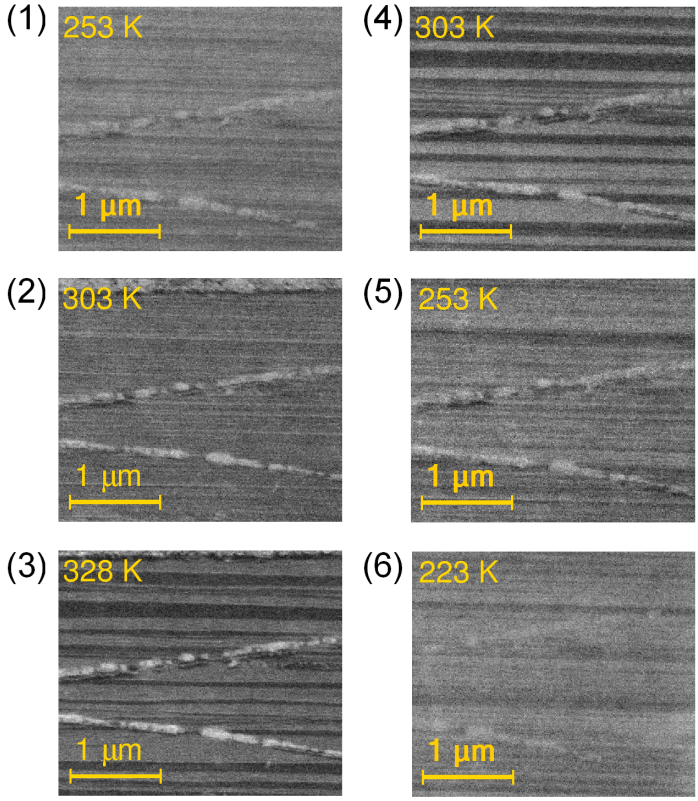

Fig. 5: SEM micrographs indicating the changes of the *a/b* laminate with temperature upon heating (1-3) and cooling (4-6). Numbers in brackets correspond to the points marked in Fig 4.

Following the SEM study of the transition from *incommensurate* to *commensurate* state and the thermal hysteresis, we measured the temperature evolution of electrical resistivity. We subtracted the linear metallic contribution (determined from the region of commensurate modulation) to make the non-linear contribution apparent, Fig. 6. The full measurement in absolute values is included in the inset in Fig. 6. The measurement was fully repeatable. The changes in resistivity are clearly visible with the temperatures matching closely those from the diffraction experiments – reflecting the transformations between the *incommensurate* and *commensurate* modulated 10M martensite. The detected increase in resistivity during the transformation from incommensurate to commensurate 10M martensite is about 1 % but well apparent. For context, the 10M martensite – cubic austenite transition with the same martensite orientation at the beginning leads to about 20 % resistivity increase (not shown). Despite the relatively small magnitude of change, our measurement unarguably indicates the gradual changes in conductive properties during the temperature evolution of 10M martensite. During heating up from 324 K (until austenite) the dependence stabilised with no tracks of hysteresis.

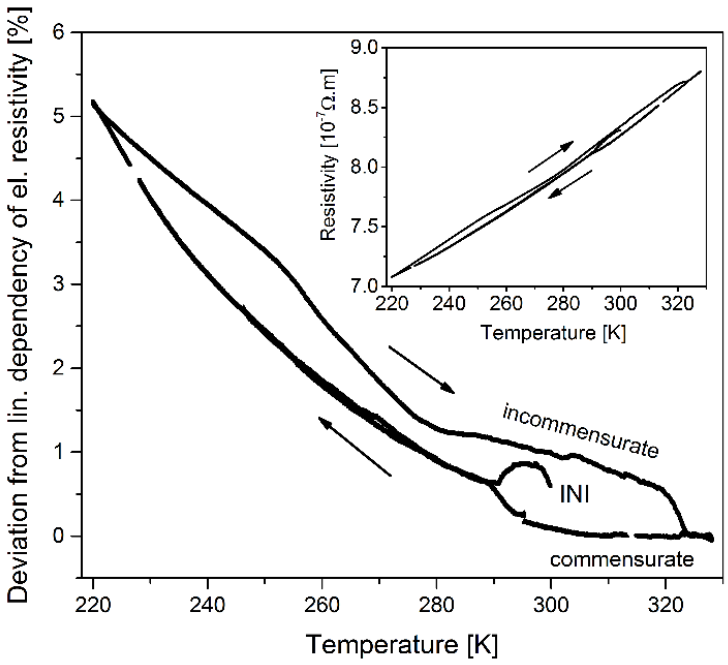

Fig. 6: Deviation from the linear dependency of electrical resistivity as a function of temperature. The points marked INI correspond to the initial undefined state of the sample. Inset: Temperature evolution of electrical resistivity in the region of hysteresis.

3.3 Resonant ultrasound spectroscopy

To investigate the possible changes of the microstructure and elastic constants, we performed RUS measurements. The sample (first in the as-cut condition and then in the field-cooled condition) was measured along a 322 K → 224 K → 325 K temperature cycle, as described in subsection 2.3. Fig. 7 shows the spectra for the as-cut condition at 322 K before (start) and after (end) the temperature cycle and the spectra for 256 K along the heating and cooling runs, respectively. The spectrum at 322 K indicated and extremely strong damping in the material [77], with no significant peak above approximately 250 kHz and a few mutually overlapping peaks below this frequency. Among them, the maxima of only two peaks can be clearly localized. However, the frequencies of these peaks are exactly the same before and after the cooling-heating cycle, which proves that the microstructure and elastic properties are completely reversible. A much higher number of peaks were detected for the spectra at 256 K, indicating much lower damping. The measured spectra for the cooling run and the heating run were very different, agreeing with the expected hysteretic behavior revealed by the diffraction and resistivity measurements.

The differences between the cooling and heating runs are clearly seen in Fig. 8, showing the evolutions of the chosen traced resonant peaks for the *a)* as-cut and *b)* field-cooled conditions. For both conditions, the spectra were initially strongly damped, with few detectable peaks exhibiting a weak and smooth temperature dependence. During cooling, at approximately 290 K, the df/dT slope abruptly changed for all modes and their frequencies started to increase rapidly, accompanied by a significant decrease in damping. In the heating run, the frequencies dropped rapidly down at approximately 320 K associated again with a sharp change of the df/dT slope.

Importantly, for both sample conditions, as-cut and field cooled, there is no discontinuous change in the spectrum at any temperature, i.e., there are always several resonant modes that can be traced even over the temperature intervals where the character of the spectrum significantly changes. This means that there are no discontinuous changes of the microstructure or the elastic constants – such changes would indicate the

presence of a first-order phase transition. The fact that the spectra for both sample conditions have a very similar character proves that the observed behavior is intrinsic to the material itself, not to the common twin boundaries that are numerous in the as-cut condition but nearly absent in the field-cooled condition. On the other hand, some differences between these two spectra suggest that the changes are specific to straining of the material along some specific crystallographic directions. In the polytwinned state, these directions are differently oriented in different domains, which means a more complex evolution of the spectrum.

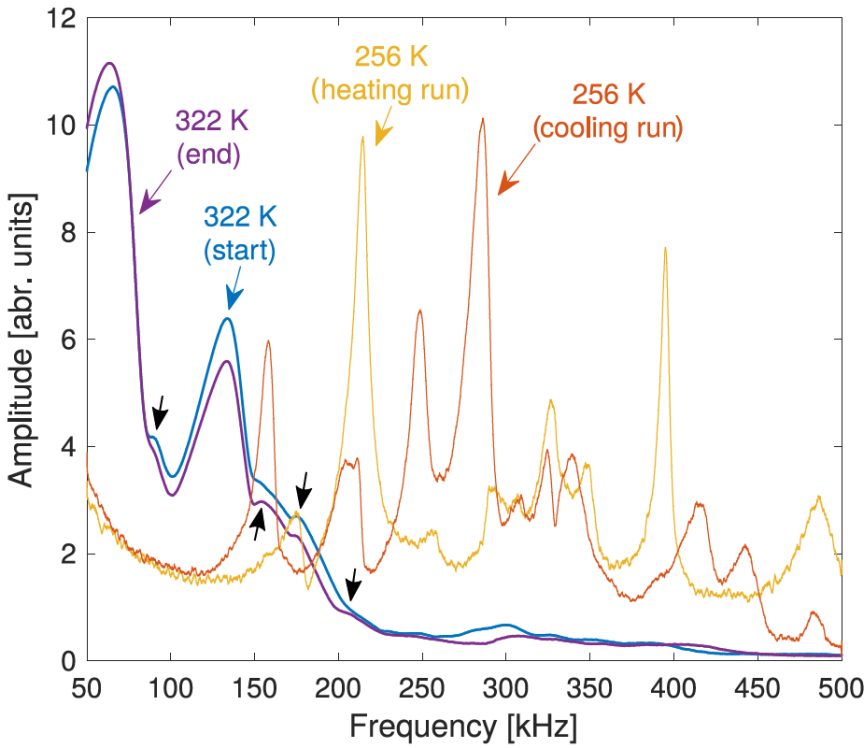

Fig. 7: Comparison of RUS spectra of as-cut sample at 256 K and 322 K. The fine features indicated for 322 K by the black arrows may be additional resonant peaks fully merged with the extremely broad peaks of the two dominant modes. The slightly worse signal-to-noise ratio for 256 K data was caused by a decreased intensity of the probe laser beam reflecting from the surface of the sample, most probably owing to slight changes of the shape of the sample or its surface relief at low temperatures.

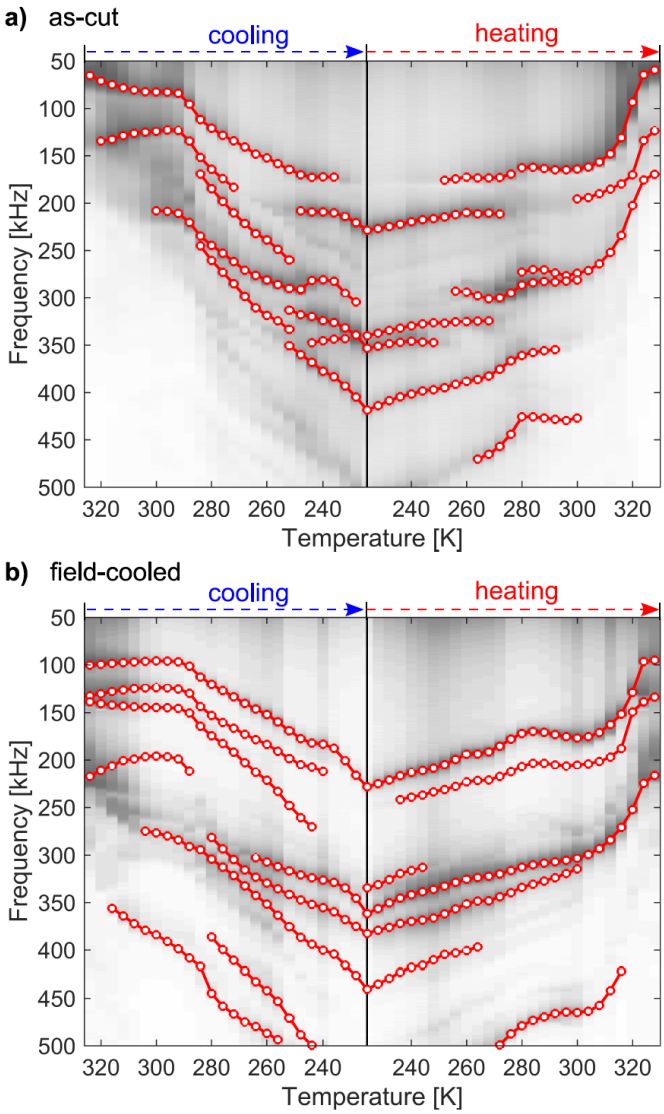

Fig. 8: Temperature evolution of RUS resonant spectrum (the grayscale represents the amplitude of vibrations) for the a) as-cut and b) field-cooled sample. The red open circles mark the manually traced individual resonant peaks.

For the field-cooled sample, one resonant mode could be traced throughout the whole temperature cycle. This enabled us to quantify the changes of the elasticity by calculating an effective elastic modulus representing this mode and its evolution with temperature. Using the scanning laser-Doppler interferometry [72], this mode was identified as a simple bending mode (the modal shape is shown in the inset in Fig. 9). Thus, the corresponding mode-specific elastic modulus can be for each temperature calculated as a Young's modulus of an isotropic sample having the same resonant frequency for this mode. Such a calculation is possible only for the lowest modes where the modal shapes are nearly material-independent [78], and for plate-like samples, where the lowest modes are dominantly bending modes with frequencies dominantly sensitive to Young's moduli.

The resulting hysteretic dependence of the modulus is shown in Fig. 9. At ~ 300 K, the values of Young's modulus, E, corresponding to the heating and cooling runs differ more than three times. Significant changes of the dE/dT slope are observed at 290 K during the cooling run, and then at ~ 280 K and above 320 K during the heating run, corresponding to the hysteresis of q (Fig. 4), twin refinement (Fig. 5), and electrical resistivity

(Fig. 6). Altogether, the Young's modulus stiffens more than five times along the thermal cycle. This is, however, not surprising, as the soft shearing modes in martensite are expected to stiffen significantly with increasing distance from the transition temperature [61]. More surprising is that this stiffening does not appear in the nearest vicinity of the transition temperature, i.e., at the beginning of the cooling run. Instead, the observed bending mode is rather weakly softening down to 290 K, where a stiffening is triggered at the start of the evolution of the non-commensurate structure.

Finally, we point out that all traced resonant frequencies for both samples exhibit, in some temperature intervals, very similar trends as the frequency of the above discussed one mode. This means that the significant stiffening (five times between 322 K and 224 K) can be understood as representative for the bending stiffness of the whole material. As the lowest resonant modes in RUS for strongly anisotropic materials are dominantly dependent on the softest shear moduli [79], we can conclude that these softest shear moduli exhibit very strong stiffening along the commensurate-to-incommensurate transition path.

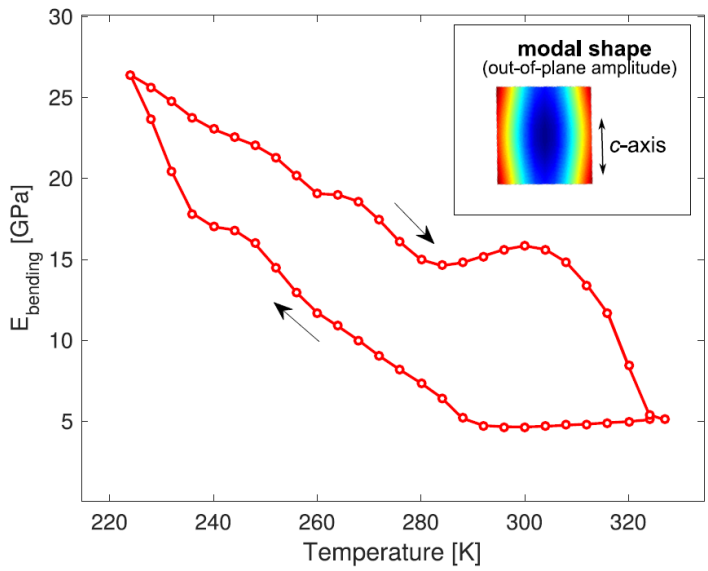

Fig. 9: Temperature evolution of an effective (mode-specific) elastic modulus for the field-cooled sample, calculated from the temperature evolution of the lowest detected resonant mode. The inset shows the corresponding modal shape and its orientation with respect to the dominant *c*-axis direction in the sample.

4. Discussion

The investigation of structural, elastic, and electrical transport properties was employed to probe into the ambiguous nature of 10M modulated martensite formed in $Ni_{50}Mn_{27}Ga_{22}Fe_1$ single crystal. All investigated properties evolved significantly in the temperature region preceding the intermartensitic transformation. All used methods detected a similar hysteretic behaviour. The detailed analysis of the modulation satellites and the nonlinear effects revealed by the electrical and elastic measurements contradicts the assumption of invariable martensite phases with abrupt intermartensitic transformations between them, although some major characteristics of the 10M phase are about the same in the whole temperature region of 10M phase stability (e.g., the crystallographic unit cell). The observed behaviour rather follows the model of continuous evolution of irregular nanotwinning in 10M and 14M martensite suggested by Benešová et al. [56].

The nanotwinning is further supported by the following facts: (i) Although the wave modulation concept describes well the structure and its evolution with temperature, the presence of modulation satellites of high order (up to at least 5th order, which is even more than three orders of modulation satellites reported by Fukuda et al. [42] and Mariager et al. [36] in Ni-Mn-Ga; measured as peaks of high intensity) is very uncommon (if possible at all) in the X-ray and neutron crystallography. Hence, irregular nanotwinning should be addressed in the future. (ii) The refining of the *a*/*b* twin laminate is observed up to nanosize twins accompanied by transition to incommensurate modulation, which may be understood as a precursor effect for the intermartensitic transition [56]. (iii) The anomalous increase in electrical resistivity during the transition from *commensurate* to *incommensurate* 10M modulated structure can be explained by additional nanotwinning and formation of many new stacking faults, both behaving as obstacles for electronic transport.

Appearance of strong extra peaks in the diffraction pattern suggests the mixture of different phases might occur in the temperature region of the incommensurate 10M martensite. Even though we did not observe any other known phase on the mesoscopic or macroscopic scale (the measured diffraction patterns did not represent the direct sum of the contributions from the possible commensurate 10M, 14M, NM or austenite phases), the new phase can also appear only on the nanoscale as a part of the nanotwinned structure, agreeing with the nanotwinning concept. Such phase would not be detectable directly by conventional XRD and ND diffraction experiments.

The RUS results showed that the commensurate phase has some very soft shearing modes that are significantly stiffening with increasing incommensurateness. Furthermore, the soft modes in the commensurate phase are strongly dissipative, causing high damping of the RUS spectrum. Both these facts suggest that the commensurate structure is much less stable than the incommensurate one. Thus, it turns out that the commensurate state may be just a metastable form of 10M martensite that appears only close to the martensitic transition temperature, but tends to transform into a more irregular but more stable structure. Furthermore, the soft elastic moduli (represented here by the mode-specific modulus shown in Fig. 9) exhibit steep stiffening upon cooling, even relatively close to the intermartensitic transition temperature. In other words, the intermartensitic transition is probably not preceded by any precursor softening, i.e., this transition does not appear to be mediated by acoustic phonons. Instead, all results indicate that the intermartensitic (10M→14M) transition is preceded by an increasing disorder (stacking faults, incommensurateness, a/b twinning) in the 10M structure, which is again very consistent with the model of Benešová et al. [56].

5. Conclusions

Structural evolution within the 10M modulated martensite of a $Ni_{50}Mn_{27}Ga_{22}Fe_1$ single crystal was found and investigated using XRD and ND. Following the conventional wave-like modulation concept, the modulation vector changes from *commensurate* $\mathbf{q} = 0.400\ \mathbf{g}_{110}$ to *incommensurate* and subsequently to *pseudo-commensurate* ($\mathbf{q} = 0.428(2)\ \mathbf{g}_{110} \approx (3/7)\ \mathbf{g}_{110}$) phase during cooling. The evolution of the modulation vector exhibits about 60 K wide thermal hysteresis around the room temperature. Based on the neutron diffraction data, we proved that the observed development is a bulk effect. Strong higher-order diffraction satellites suggest the need for the development of an irregular nanotwinning model that could explain the measured satellite peak intensities and the presence of the critical value of $\mathbf{q} \approx (3/7)\ \mathbf{g}_{110}$ near the 10M→14M intermartensitic transformation, also recorded in previous investigations. Irregular nanotwinning is also indicated by the changes in the *a*/*b* nanolaminate directly observed by the SEM.

The diffraction-based observation of the hysteretic transition between the commensurate and incommensurate modulated 10M martensite is further supported by electrical resistivity measurement and resonant ultrasound spectroscopy. The soft elastic moduli exhibit steep stiffening upon cooling and corresponding reverse hardening upon heating, with hysteresis corresponding to that observed for **q**. Altogether, the simultaneous changes of multiple physical properties indicate a gradual phase transformation, where the *commensurate* 10M represents a metastable phase and the structure continuously evolves into the *incommensurate* 10M martensite structure.

Our findings contradict the assumption of invariable martensite phases with abrupt intermartensitic transformations between them and rather imply the continuous evolution of irregular nanotwinning.

Noteworthy, owing to the hysteresis, the 10M martensite of $Ni_{50}Mn_{27}Ga_{22}Fe_1$ alloy can be prepared in the *commensurate* or *incommensurate* state at the same temperature using the appropriate heating/cooling procedure. At the same time, by controlling the Fe content in the alloy, the temperatures where the hysteresis appears can be set to the vicinity of room temperature. Hence, this approach might be further utilized to study the effect of commensurateness on the mobility of twin boundaries and to facilitate further the understanding of the nature of modulation.

Acknowledgements

This work was supported by the Czech Science Foundation (Czech Republic) [grant numbers 19-09882S and H.S. by 20-12624S] and by Operational Programme Research, Development and Education financed by the European Structural and Investment Funds and the Czech Ministry of Education, Youth and Sports [project number SOLID21 CZ.02.1.01/0.0/0.0/16_019/0000760 and MATFUN CZ.02.1.01/0.0/0.0/15_003/0000487]. P.V. thanks for the support by the Grant Agency of the Czech Technical University in Prague, [grant number SGS19/190/OHK4/3T/14]. The work of A.S. was supported by the Strategic Research Council (SRC) of Finland [grant number 313349]. We acknowledge the Institut Laue-Langevin for the provision of neutron radiation facilities. The work was supported within the project LTT20014 financed by the Ministry of Education, Youth and Sports, Czech Republic.

Authors kindly thank L. Klimša for performing the SEM observations, M. Rameš for the DC susceptibility measurement, M. Vališka for assistance with some of the ND experiments, and J. Drahokoupil and O. Pacherová for assistance with some of the XRD experiments.

References

[1] Krenke T, Acet M, Wassermann E F, Moya X, Mañosa L and Planes A 2005 Martensitic transitions and the nature of ferromagnetism in the austenitic and martensitic states of Ni-Mn-Sn alloys *Phys. Rev. B - Condens. Matter Mater. Phys.* **72** 014412

[2] Çakir A, Righi L, Albertini F, Acet M and Farle M 2015 Intermartensitic transitions and phase stability in Ni50Mn50-xSnx Heusler alloys *Acta Mater.* **99** 140–9

[3] Liu Z H, Liu H, Zhang X X, Zhang M, Dai X F, Hu H N, Chen J L and Wu G H 2004 Martensitic transformation and magnetic properties of Heusler alloy Ni-Fe-Ga ribbon *Phys. Lett. Sect. A Gen. At. Solid State Phys.* **329** 214–20

[4] Entel P, Siewert M, Gruner M E, Herper H C, Comtesse D, Arróyave R, Singh N, Talapatra A, Sokolovskiy V V, Buchelnikov V D, Albertini F, Righi L and Chernenko V A 2013 Complex magnetic ordering as a driving mechanism of multifunctional properties of Heusler alloys from first principles *Eur. Phys. J. B* **86** 65

[5] Felser C, Wollmann L, Chadov S, Fecher G H and Parkin S S P 2015 Basics and prospective of magnetic Heusler compounds *APL Mater.* **3** 041518

[6] Sutou Y, Imano Y, Koeda N, Omori T, Kainuma R, Ishida K and Oikawa K 2004 Magnetic and martensitic transformations of NiMnX(X=In, Sn, Sb) ferromagnetic shape memory alloys *Appl. Phys. Lett.* **85** 4358–60

[7] Oikawa K, Ota T, Ohmori T, Tanaka Y, Morito H, Fujita A, Kainuma R, Fukamichi K and Ishida K 2002 Magnetic and martensitic phase transitions in ferromagnetic Ni-Ga-Fe shape memory alloys *Appl. Phys. Lett.* **81** 5201–3

[8] Oikawa K, Ota T, Sutou Y, Ohmori T, Kainuma R and Ishida K 2002 Magnetic and martensitic

phase transformations in a Ni54Ga27Fe19 alloy *Mater. Trans.* **43** 2360–2

[9] Hamilton R F, Sehitoglu H, Efstathiou C and Maier H J 2007 Inter-martensitic transitions in Ni-Fe-Ga single crystals *Acta Mater.* **55** 4867–76

[10] Wilson S A, Jourdain R P J, Zhang Q, Dorey R A, Bowen C R, Willander M, Wahab Q U, Willander M, Al-hilli S M, Nur O, Quandt E, Johansson C, Pagounis E, Kohl M, Matovic J, Samel B, van der Wijngaart W, Jager E W H, Carlsson D, Djinovic Z, Wegener M, Moldovan C, Abad E, Wendlandt M, Rusu C and Persson K 2007 New materials for micro-scale sensors and actuators. An engineering review *Mater. Sci. Eng. R Reports* **56** 1–129

[11] Smith A R, Saren A, Järvinen J and Ullakko K 2015 Characterization of a high-resolution solid-state micropump that can be integrated into microfluidic systems *Microfluid. Nanofluidics* **18** 1255–63

[12] Kohl M, Gueltig M, Pinneker V, Yin R, Wendler F and Krevet B 2014 Magnetic shape memory microactuators *Micromachines* **5** 1135–60

[13] Martynov V V and Kokorin V V 1992 The crystal structure of thermally- and stress-induced Martensites in Ni2MnGa single crystals *J. Phys III Fr.* **2** 739–49

[14] Martynov V V 1995 X-Ray Diffraction Study of Thermally and Stress-Induced Phase Transformations in Single Crystalline Ni-Mn-Ga Alloys *Le J. Phys. IV* **05** C8-91-C8-99

[15] Brown P J, Neumann K-U, Ziebeck K R A, Bargawi A Y and Crangle J 1999 Direct observation of a band Jahn-Teller effect in the martensitic phase transition of Ni 2 MnGa Redistribution of magnetization in the martensitic transitionof V3Si Direct observation of a band Jahn–Teller effect in the martensitic phase transition of Ni *J. Phys. Condens. Matter* **11** 4715–22

[16] Straka L, Heczko O, Seiner H, Lanska N, Drahokoupil J, Soroka A, Fähler S, Hänninen H and Sozinov A 2011 Highly mobile twinned interface in 10 M modulated Ni-Mn-Ga martensite: Analysis beyond the tetragonal approximation of lattice *Acta Mater.* **59** 7450–63

[17] Lanska N, Söderberg O, Sozinov A, Ge Y, Ullakko K and Lindroos V K 2004 Composition and temperature dependence of the crystal structure of Ni-Mn-Ga alloys *J. Appl. Phys.* **95** 8074–8

[18] Vasil'ev A N, Bozhko A D, Khovailo V V, Dikshtein I E, Shavrov V G, Buchelnikov V D, Matsumoto M, Suzuki S, Takagi T and Tani J 1999 Structural and magnetic phase transitions in shape-memory alloys (formula presented) *Phys. Rev. B - Condens. Matter Mater. Phys.* **59** 1113–20

[19] Khovailo V V, Oikawa K, Wedel C, Takagi T, Abe T and Sugiyama K 2004 Influence of intermartensitic transitions on transport properties of Ni2.16Mn0.84Ga alloy *J. Phys. Condens. Matter* **16** 1951–61

[20] Heczko O, Straka L and Seiner H 2013 Different microstructures of mobile twin boundaries in 10 M modulated Ni-Mn-Ga martensite *Acta Mater.* **61** 622–31

[21] Ullakko K, Huang J K, Kantner C and Handley R C O 1996 Large magnetic-field-induced strains in Ni2MnGa single crystals *Appl. Phys. Lett.* **69** 1966–8

[22] Heczko O, Sozinov A and Ullakko K 2000 Giant field-induced reversible strain in magnetic shape memory NiMnGa alloy *IEEE Trans. Magn.* **36** 3266–8

[23] Heczko O, Kopecký V, Sozinov A and Straka L 2013 Magnetic shape memory effect at 1.7 K *Appl. Phys. Lett.* **103** 072405

[24] Okamoto N, Fukuda T and Kakeshita T 2008 Temperature dependence of rearrangement of martensite variants by magnetic field in 10M, 14M and 2M martensites of Ni-Mn-Ga alloys *Mater. Sci. Eng. A* **481**–**482** 306–9

[25] Kaufmann S, Niemann R, Thersleff T, Rößler U K, Heczko O, Buschbeck J, Holzapfel B, Schultz L and Fähler S 2011 Modulated martensite: Why it forms and why it deforms easily *New J. Phys.* **13**

[26] Seiner H, Straka L and Heczko O 2014 A microstructural model of motion of macro-twin interfaces in Ni-Mn-Ga 10 M martensite *J. Mech. Phys. Solids* **64** 198–211

[27] Müllner P 2019 Twinning stress of type I and type II deformation twins *Acta Mater.* **176** 211–9

[28] Bodnárová L, Zelený M, Sedlák P, Straka L, Heczko O, Sozinov A and Seiner H 2020 Switching the soft shearing mode orientation in Ni-Mn-Ga non-modulated martensite by Co and Cu doping *Smart Mater. Struct.* **29** 045022

[29] Sozinov A, Lanska N, Soroka A and Zou W 2013 12% magnetic field-induced strain in Ni-Mn-Ga-based non-modulated martensite *Appl. Phys. Lett.* **102** 021902

[30] Webster P J, Ziebeck K R A, Town S L and Peak M S 1984 Magnetic order and phase transformation in Ni2MnGa *Philos. Mag. B Phys. Condens. Matter; Stat. Mech. Electron. Opt. Magn. Prop.* **49** 295–310

[31] Singh S, Bednarcik J, Barman S R, Felser C and Pandey D 2015 Premartensite to martensite transition and its implications for the origin of modulation in N i2MnGa ferromagnetic shape-memory alloy *Phys. Rev. B - Condens. Matter Mater. Phys.* **92** 054112

[32] Khachaturyan A G and Shatalov G A 1969 Theory of Macroscopic Periodicity for a Phase Transition in the Solid State *Zh. Eksp. Teor. Fiz* **29** 1037–45

[33] Khachaturyan A G, Shapiro S M and Semenovskaya S 1991 Adaptive phase formation in martensitic transformation *Phys. Rev. B* **43** 10832–43

[34] Kaufmann S, Rößler U K, Heczko O, Wuttig M, Buschbeck J, Schultz L and Fähler S 2010 Adaptive modulations of martensites *Phys. Rev. Lett.* **104** 145702

[35] Pons J, Chernenko V A, Santamarta R and Cesari E 2000 Crystal structure of martensitic phases in Ni-Mn-Ga shape memory alloys *Acta Mater.* **48** 3027–38

[36] Mariager S O, Huber T and Ingold G 2014 The incommensurate modulations of stoichiometric Ni2MnGa *Acta Mater.* **66** 192–8

[37] De Wolff P M, Janssen T and Janner A 1981 The superspace groups for incommensurate crystal structures with a one-dimensional modulation *Acta Crystallogr. Sect. A* **37** 625–36

[38] Janssen T, Janner A, Looijenga-Vos A and de Wolff P M 2006 Incommensurate and commensurate modulated structures *International Tables for Crystallography* pp 907–55

[39] Righi L, Albertini F, Pareti L, Paoluzi A and Calestani G 2007 Commensurate and incommensurate "5M" modulated crystal structures in Ni-Mn-Ga martensitic phases *Acta Mater.* **55** 5237–45

[40] Righi L, Albertini F, Paoluzi A, Fabbrici S, Villa E, Calestani G and Besseghini S 2010 Incommensurate and commensurate structural modulation in martensitic phases of FSMA *Mater. Sci. Forum* **635** 33–41

[41] Singh S, Barman S R and Pandey D 2015 Incommensurate modulations in stoichiometric Ni2MnGa ferromagnetic shape memory alloy: An overview *Zeitschrift fur Krist.* **230** 13–22

[42] Fukuda T, Kushida H, Todai M, Kakeshita T and Mori H 2009 Crystal structure of the martensite phase in the ferromagnetic shape memory compound Ni2MnGa studied by electron diffraction *Scr. Mater.* **61** 473–6

[43] Çakir A, Acet M, Righi L, Albertini F and Farle M 2015 Characteristics of 5M modulated martensite in Ni-Mn-Ga magnetic shape memory alloys *AIP Adv.* **5** 097222

[44] Niemann R and Fähler S 2017 Geometry of adaptive martensite in Ni-Mn-based Heusler alloys *J. Alloys Compd.* **703** 280–8

[45] Gruner M E, Niemann R, Entel P, Pentcheva R, Rößler U K, Nielsch K and Fähler S 2018 Modulations in martensitic Heusler alloys originate from nanotwin ordering *Sci. Rep.* **8** 1–12

[46] Zhdanov G S 1945 The numerical symbol of close packing of spheres and its application in the theory of close packings *Compt. Rend. Acad. Sci. URSS* **48** 39–42

[47] Zelený M 2018 Nanotwinning and modulation of martensitic structures in Ni2MnGa alloy: An ab

initio Study *Acta Phys. Pol. A* **134** 658–61

[48] Beran L, Cejpek P, Kulda M, Antos R, Holy V, Veis M, Straka L and Heczko O 2015 Optical and magneto-optical studies of martensitic transformation in Ni-Mn-Ga magnetic shape memory alloys *J. Appl. Phys.* **117** 17A919

[49] Wang Y U 2006 Diffraction theory of nanotwin superlattices with low symmetry phase *Phys. Rev. B - Condens. Matter Mater. Phys.* **74** 1–4

[50] Wang Y U 2007 Diffraction theory of nanotwin superlattices with low symmetry phase: Application to rhombohedral nanotwins and monoclinic MA and MB phases *Phys. Rev. B - Condens. Matter Mater. Phys.* **76** 1–11

[51] Straka L, Drahokoupil J, Veřtát P, Kopeček J, Zelený M, Seiner H and Heczko O 2017 Orthorhombic intermediate phase originating from {110} nanotwinning in Ni50.0Mn28.7Ga21.3 modulated martensite *Acta Mater.* **132** 335–44

[52] Straka L, Drahokoupil J, Veřtát P, Zelený M, Kopeček J, Sozinov A and Heczko O 2018 Low temperature a/b nanotwins in Ni50Mn25+xGa25−x Heusler alloys *Sci. Rep.* **8** 11943

[53] Ge Y, Zárubová N, Heczko O and Hannula S P 2015 Stress-induced transition from modulated 14M to non-modulated martensite in Ni-Mn-Ga alloy *Acta Mater.* **90** 151–60

[54] Ball J M and James R D 1989 Fine Phase Mixtures as Minimizers of Energy *Analysis and Continuum Mechanics* ed S S Antman, H Brezis, B D Coleman, M Feinberg, J A Nohel and W P Ziemer (Berlin, Heidelberg: Springer Berlin Heidelberg) pp 647–86

[55] Schwabe S, Niemann R, Backen A, Wolf D, Damm C, Walter T, Seiner H, Heczko O, Nielsch K and Fähler S 2021 Building Hierarchical Martensite *Adv. Funct. Mater.* **31** 2005715

[56] Benešová B, Frost M, Kampschulte M, Melcher C, Sedlák P and Seiner H 2015 Incommensurateness in nanotwinning models of modulated martensites *Phys. Rev. B - Condens. Matter Mater. Phys.* **92** 180101

[57] Migliori A, Sarrao J L, Visscher W M, Bell T M, Lei M, Fisk Z and Leisure R G 1993 Resonant ultrasound spectroscopic techniques for measurement of the elastic moduli of solids *Phys. B Phys. Condens. Matter* **183** 1–24

[58] Leisure R G and Willis F A 1997 Resonant ultrasound spectroscopy *J. Phys. Condens. Matter* **9** 6001–29

[59] Nakamura N, Nakashima T, Oura S, Ogi H and Hirao M 2010 Resonant-ultrasound spectroscopy for studying annealing effect on elastic constant of thin film *Ultrasonics* **50** 150–4

[60] Landa M, Sedlák P, Šittner P, Seiner H and Novák V 2007 Temperature dependence of elastic properties of cubic and orthorhombic phases in Cu-Al-Ni shape memory alloy near their stability limits *Mater. Sci. Eng. A* **462** 320–4

[61] Nakanishi N 1980 Elastic constants as they relate to lattice properties and martensite formation *Prog. Mater. Sci.* **24** 143–265

[62] Straka L and Heczko O 2003 Magnetic anisotropy in Ni-Mn-Ga martensites *J. Appl. Phys.* **93** 8636

[63] Chen F, Wang H B, Zheng Y F, Cai W and Zhao L C 2005 Effect of Fe addition on transformation temperatures and hardness of NiMnGa magnetic shape memory alloys *J. Mater. Sci.* **40** 219–21

[64] Cherechukin A A, Dikshtein I E, Ermakov D I, Glebov A V., Koledov V V., Kosolapov D A, Shavrov V G, Tulaikova A A, Krasnoperov E P and Takagi T 2001 Shape memory effect due to magnetic field-induced thermoelastic martensitic transformation in polycrystalline Ni-Mn-Fe-Ga alloy *Phys. Lett. Sect. A Gen. At. Solid State Phys.* **291** 175–83

[65] Soto-Parra D E, Moya X, Manosa L, Planes A, Flo Es-Zuniga H, Alvarado-Hernandez F, Ochoa-Gamboa R A, Matutes-Aquino J A and Rios-Jara D 2010 Fe and Co selective substitution in Ni2MnGa: Effect of magnetism on relative phase stability *Philos. Mag.* **90** 2771–92

[66] Li C M, Luo H Bin, Hu Q M, Yang R, Johansson B and Vitos L 2011 Site preference and elastic properties of Fe-, Co-, and Cu-doped Ni 2MnGa shape memory alloys from first principles *Phys. Rev. B - Condens. Matter Mater. Phys.* **84** 024206

[67] Reimer L 2000 Scanning Electron Microscopy: Physics of Image Formation and Microanalysis, Second Edition *Meas. Sci. Technol.* **11** 1826–1826

[68] Heczko O, Klimša L and Kopeček J 2017 Direct observation of a-b twin laminate in monoclinic five-layered martensite of Ni-Mn-Ga magnetic shape memory single crystal *Scr. Mater.* **131** 76–9

[dataset][69] Klicpera M, Fabelo Rosa O R, Heczko O, Straka L and Vertat P 2018 Intermartensitic transformations and search for the ground state in Ni-Mn-Ga single crystals exhibiting the magnetic shape memory effect

[dataset][70] Klicpera M, Fabelo Rosa O R, Vertat P, Heczko O and Straka L 2019 Investigation of commensurate-incommensurate structure modulation transitions in Ni-Mn-Ga-Fe martensite

[71] Veřtát P and Drahokoupil J 2018 Fitexc – Diffraction Profile Fitting Program Run in Ms Excel *Acta Polytech. CTU Proc.* **17** 20

[72] Sedlák P, Seiner H, Zídek J, Janovská M and Landa M 2014 Determination of All 21 Independent Elastic Coefficients of Generally Anisotropic Solids by Resonant Ultrasound Spectroscopy: Benchmark Examples *Exp. Mech.* **54** 1073–85

[73] Salje E K H, Carpenter M A, Nataf G F, Picht G, Webber K, Weerasinghe J, Lisenkov S and Bellaiche L 2013 Elastic excitations in BaTiO3 single crystals and ceramics: Mobile domain boundaries and polar nanoregions observed by resonant ultrasonic spectroscopy *Phys. Rev. B - Condens. Matter Mater. Phys.* **87** 014106

[74] Kabla M, Seiner H, Musilova M, Landa M and Shilo D 2014 The relationships between sputter deposition conditions, grain size, and phase transformation temperatures in NiTi thin films *Acta Mater.* **70** 79–91

[75] Veřtát P, Straka L, Drahokoupil J and Heczko O 2018 Study of 10M' nanotwinned phase in the vicinity of martensitic transformation in Ni–Mn–Ga magnetic shape memory alloy *Acta Phys. Pol. A* **134** 859–62

[76] Chulist R, Straka L, Seiner H, Sozinov A, Schell N and Tokarski T 2019 Branching of {110) twin boundaries in five-layered Ni-Mn-Ga bent single crystals *Mater. Des.* **171** 107703

[77] Sumino Y, Ohno I, Goto T and Kumazawa M 1976 Measurement of elastic constants and internal frictions on single-crystal mgo by rectangular parallelepiped resonance *J. Phys. Earth* **24** 263–73

[78] Demarest H H 1971 Cube-Resonance Method to Determine the Elastic Constants of Solids *J. Acoust. Soc. Am.* **49** 768–75

[79] Landa M, Sedlák P, Seiner H, Heller L, Bicanová L, Šittner P and Novák V 2009 Modal resonant ultrasound spectroscopy for ferroelastics *Appl. Phys. A Mater. Sci. Process.* **96** 557–67